

Underwater Image Enhancement via Principal Component Fusion of Foreground and Background

Weidong Zhang^{ID}, Senior Member, IEEE, Qingmin Liu^{ID}, Yikun Feng, Lei Cai^{ID}, and Peixian Zhuang^{ID}, Member, IEEE

Abstract—Underwater imaging systems have evolved into essential hardware equipment for developing and utilizing marine resources. However, the complex underwater physical environment has often led to severe quality degradation of underwater visual perception. To address these issues, we design a principal component fusion method of foreground and background to enhance an underwater image, named PCFB. Specifically, we present a color balance-guided color correction strategy to remove color distortion issues that equalize the pixel values of the a and b channels of the CIELab color model. Subsequently, we implement a percentile maximum-based contrast enhancement strategy and a multilayer transmission map estimated dehazing strategy on the color-corrected image to yield the contrast-enhanced foreground and dehazed background sub-images. Finally, we employ a principal component analysis fusion method to reconstruct a high-visibility underwater image by integrating the advantages of the foreground contrast-enhanced sub-image and the background dehazed

Manuscript received 17 November 2023; revised 4 March 2024; accepted 7 June 2024. Date of publication 11 June 2024; date of current version 27 November 2024. This work was supported in part by the Natural Science Foundation of Henan Province under Grant 232300420428; in part by the Key Specialized Research and Development Program of Science and Technology of Henan Province under Grant 242102210075, Grant 232102210018, and Grant 242102211096; in part by the Teacher Education Curriculum Reform Research of Henan Province under Grant 2024-JSJYYB-099; in part by the National Natural Science Foundation of China under Grant 62171252 and Grant 61701245; in part by the Key Research and Development Program of Henan Province under Grant 241111211800 and Grant 231111220700; and in part by the Fundamental Research Funds for the Central Universities under Grant 00007764. This article was recommended by Associate Editor H. Sun. (*Corresponding author: Peixian Zhuang.*)

Weidong Zhang is with the Postdoctoral Innovation Practice Base, Henan Institute of Science and Technology, Xinxiang 453003, China, also with the Postdoctoral Workstation, Henan Bainong Seed Industry Company Ltd., Henan Institute of Science and Technology, Xinxiang 453003, China, also with the School of Information Engineering and the Institute of Computer Applications, Henan Institute of Science and Technology, Xinxiang 453003, China, and also with the College of Electrical and Information Engineering, Zhengzhou University, Zhengzhou 450001, China (e-mail: zwd_wd@163.com).

Qingmin Liu is with the School of Information Engineering and the Institute of Computer Applications, Henan Institute of Science and Technology, Xinxiang 453003, China (e-mail: liuqm0601@163.com).

Yikun Feng is with the Adam Smith Business School, University of Glasgow, G12 8QQ Glasgow, U.K. (e-mail: 2569413f@student.gla.ac.uk).

Lei Cai is with the School of Artificial Intelligence, Henan Institute of Science and Technology, Xinxiang 453003, China (e-mail: cailei2014@126.com).

Peixian Zhuang is with the School of Automation and Electrical Engineering, University of Science and Technology Beijing, Beijing 100083, China (e-mail: zhuangpeixian0624@163.com).

This article has supplementary material provided by the authors and color versions of one or more figures available at <https://doi.org/10.1109/TCSVT.2024.3412748>.

Digital Object Identifier 10.1109/TCSVT.2024.3412748

sub-image. Comprehensive experiments on three datasets demonstrate that our PCFB surpasses state-of-the-art methods both qualitatively and quantitatively. Moreover, our PCFB exhibits outstanding generalization capabilities for addressing haze and low-light images. The code is publicly available at: https://www.researchgate.net/publication/381259520_2024-PCFB.

Index Terms—Underwater visual perception, foreground contrast-enhanced, background dehazed, principal component fusion.

I. INTRODUCTION

UNDERWATER visual quality enhancement technology significantly influences underwater archaeology, marine exploration, and underwater engineering [1], [2], [3]. Unfortunately, underwater visual images face variable quality degradation due to the complex underwater physicalization factors, which limits underwater visual perception and the performance of information acquisition [4], [5], [6]. Thus, underwater image sharpening methods are significant in the underwater vision field.

Researchers have recently proposed many underwater image enhancement methods to solve these challenges. Generally speaking, these methods can be roughly summarized as image restoration [7], [8], [9], [10], [11], [12], [13], [14], [15], [16], [17], [18], [19], image enhancement [20], [21], [22], [23], [24], [25], [26], [27], [28], [29], [30], [31], and deep learning methods [32], [33], [34], [35], [36], [37], [38], [39]. Specifically, image restoration requires many prior assumptions to make model optimization difficult. In general, image enhancement methods usually ignore the underwater image imaging model, which results in color distortion and noise amplification. Deep learning methods require a wealth of high-quality image pairs for model training. Nonetheless, acquiring sharper underwater images poses an exceptionally challenging task, significantly impeding the advancement of this research method.

In our work, we proposed a Principal Component fusion method of the Foreground and Background method improve underwater visual perception, called **PCFB**. Specifically, our PCFB comprises four primary stages: color balance-guided color correction, percentile maximum-based contrast enhancement, multilayer transmission map estimated dehazing, and principal component analysis fusion. In the first stage, we normalize the pixel values of the a and b channels of the CIELab color model and update the channels with lower average

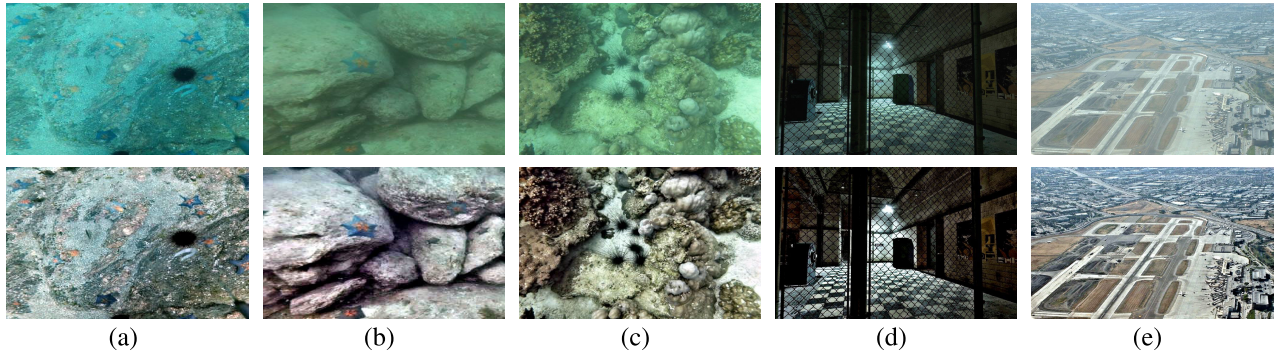


Fig. 1. **Results obtained using our PCFB method.** From left to right are degraded images (Top) from UCCS [40], UIQS [40], UIEB [32], and low-light and dehazing images from the Internet, respectively. The corresponding enhanced results (Bottom) were obtained using our PCFB method.

pixel values via a specific calculation to obtain a color-corrected image. Subsequently, we apply pixel replacement to the color-corrected image using percentiles based on a pre-determined threshold to yield a foreground contrast-enhanced sub-image. Meanwhile, we utilize the atmospheric scattering model and stratified transmittance estimation applied to the color-corrected to yield a background dehazed sub-image. Finally, we employ a principal component analysis fusion to combine the advantage features of the contrast-enhanced foreground image and the dehazed background image to obtain a clearer underwater image. Besides, Fig. 1 exhibits the processed visual result of our PCFB for low-quality underwater images with different degrees of degradation.

We underline the contributions of this work as follows.

- We introduce a simple yet effective principal component fusion method of foreground and background, which corrects underwater image color casts and enhances image contrast and preserves crucial information and texture details from the raw image. Likewise, our PCFB demonstrates strong generalization capabilities when applied to images taken in haze and low-light conditions.
- We introduce a contrast enhancement based on the percentile maximum method and a multilayer transmission map estimated dehazing method to improve the color-corrected image's contrast and clarity. Our findings demonstrate that the advantage feature fusion of the contrast-enhanced and dehazed images significantly improves underwater visual perception.
- We present a principal component analysis fusion, which computes the eigenvalues and eigenvectors from the covariance matrix of the contrast-enhanced foreground and dehazed background sub-images, which efficiently determines normalized weights derived from these values for advantage feature fusion to obtain a clearer underwater image with different image advantages.

II. RELATED WORK

Presently, researchers have put forth numerous methods to improve underwater visual perception, which can be categorized into three main groups: image restoration, image enhancement, and deep learning techniques. The overview of these methods is summarized as follows.

A. Image Restoration Methods

Image restoration methods restore a clear image by deducing and estimating the raw image information and inverting the degradation process by the underwater imaging model, which mainly contains underwater optical imaging [7], [8], [9], polarization property [10], [11], prior knowledge [12], [13], [14], [15], [19], [41], and variational model [16], [17], [18]. For example, the Jaffe-McGlamery imaging model [8] and the dark channel prior (DCP) [12] are implemented to improve underwater vision. Liang et al. [9] designed a robust DCP for multiple degradation types of images. However, it adopted a multi-prior optimization strategy, leading to complex parameter estimation and computational difficulties. Additionally, Li et al. [14] put forward a new sphere method to accurately compute the transmission map, which overcame the noise sensitivity of the transmission map in the traditional DCP and effectively removed the haze. In conclusion, these studies face limitations due to the variability and diversity of marine imaging processes and the challenges associated with model parameter optimization.

B. Image Enhancement Methods

Image enhancement methods can improve contrast, color, and clarity by adjusting the pixels and obtaining a high-quality image, which is represented by frequency domain [20], [21], [22], [23], spatial domain [24], [25], [42], color constancy [26], [27], [28], and fusion methods [29], [30], [31], [43], [44]. For instance, Li et al. [20] adopted a Gaussian difference filter and a bilateral filter to adaptively adjust the contrast and color of underwater images, effectively improving the contrast of images but ignoring image details due to insufficient consideration of the imaging model. To alleviate the issue, Zhang et al. [21] devised a new method to optimize both color and contrast, which effectively improved image contrast and texture details but had the problem of excessive noise. Li et al. [24] employed a contrast enhancement method based on color correction and detail retention, solving this challenge of color distortion and excessive noise in underwater images. Although these methods have sound effects in improving the brightness, contrast, and texture details of underwater images, some areas of the image are over-enhanced or oversaturated because the imaging mechanism is ignored.

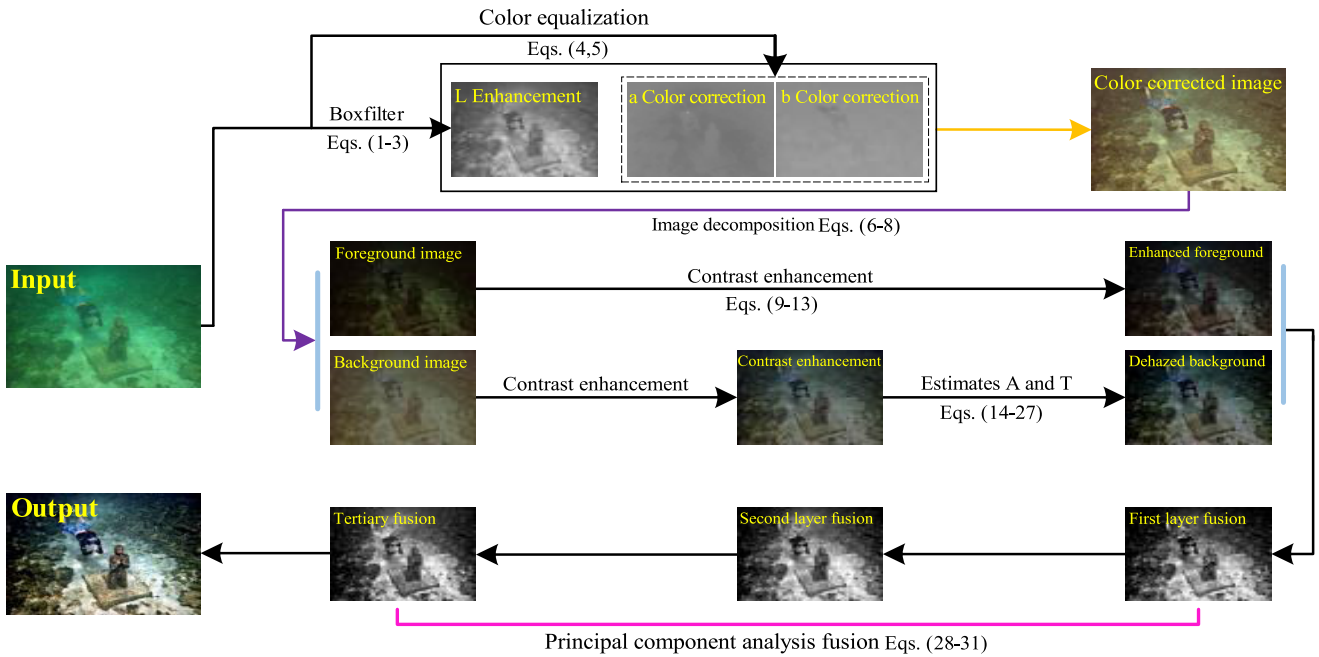


Fig. 2. **The workflow of our PCFB method.** Input an image that is color-corrected by a color balance-guided color correction method. Subsequently, two quality-improved images, named the foreground contrast-enhanced and the background dehazed sub-images, are derived from the color-balanced image, using a percentile maximum-based contrast enhancement method and a multilayer transmission map estimated dehazing method, respectively. Finally, advantage features from the foreground contrast-enhanced and the background dehazed sub-image are fused by principal component analysis.

C. Deep Learning Methods

Deep learning methods mainly explore the extraction of valuable features and learning nonlinear relations by deep network structure of deep learning, which includes primarily CNN-based [32], [33], [34], [35], [45], [46] and GAN-based methods [36], [37], [38], [39], [47]. For example, Li et al. [32] created an underwater image enhancement dataset (UIEB) and designed an underwater visual sharpening network. The efficiency of the dataset for training convolutional neural networks was verified. Besides, Li et al. [33] utilized underwater scene prior and physical models to build an underwater synthetic dataset with reference images to alleviate data scarcity, which shows good enhancement performance on the synthetic dataset and has a good effect on underwater video enhancement. Liu et al. [38] designed a dual-supervised GAN, which enhanced image brightness and corrected image color in the weakly supervised learning stage and enhanced image texture details in the intensely directed learning stage. Although deep learning techniques have demonstrated superior performance in underwater vision enhancement, they are limited to the difficulty of acquiring numerous high-quality underwater images.

III. METHODOLOGY

We detail the proposed PCFB in Fig. 2. In the color balance-guided color correction (CBCC), we adopt the box filtering and the color balance to work together to enhance the L channel and balance the pixel values of the a and b channels. Afterward, we employ the percentile maximum-based contrast enhancement strategy on the color-corrected image to obtain the foreground contrast-enhanced sub-image (FCES). Meanwhile, the multilayer transmission map estimated dehazing

technique is applied to the color-corrected image to get the background dehazed sub-image (BDSI). Finally, a high-quality result is acquired via the principal component analysis fusion strategy (PCAF).

A. Motivation

Different from land images, underwater images face more serious degradation problems [48], and traditional image enhancement techniques cannot obtain satisfactory results. Recently, the dual-histogram strategy alleviated the problem of over-enhancement or over-saturation caused by traditional histograms by separating the foreground and background of the underwater image [21]. Unfortunately, the simple processing and fusion of the foreground and background may lead to local halos or underexposure in the enhanced underwater images due to the insufficient usefulness of advantageous underwater image features.

Notably, the fusion-based method effectively mitigates the halo effect commonly observed in traditional linear fusion methods. It has gradually been applied to underwater image enhancement by integrating the advantages of different enhanced images. For example, feature map fusion [49], high- and low-frequency component fusion [50], local feature fusion [51], multi-scale fusion [52], hybrid fusion [44], etc. Although these fusion methods utilize different fusion strategies to obtain the advantage information of different enhanced versions of images, these methods are rarely considered from the perspective of image principal component information fusion. Unlike the above fusion strategies, our approach fully considers the advantages of foreground and background enhancement images. Meanwhile, we use the

principal component fusion strategy to realize the fusion of different image components using the covariance matrix of different images.

B. Color Balance-Guided Color Correction

Underwater images commonly exhibit the color deviation hue due to light absorption in the water medium. Rectifying these color variations is crucial to improving the quality of the raw underwater image. Inspired by the traditional methods of color correction [53], [54], [55], [56], [57], we propose a color balance-guided color correction method. The technique consists of two steps: 1) Localized contrast enhancement strategy for the L channel to avoid image exposure or distortion problems due to too many pixels in the local image block. 2) Pixel equalization for a and b channels to weaken the problem of loss of contour information due to light attenuation by locally equalizing the colors and details of raw underwater images.

We initially utilize the box filtering method to compute the mean and variance of the L channel in the CIELab color model. For simplicity, let's take local block B as an example. The mathematical expression for this process is as

$$N_B = \sum_{i=-r}^r \sum_{j=-r}^r 1, \quad (1)$$

$$\mathbf{I}_{\text{mean}}(x, y) = \frac{\sum_{i=-r}^r \sum_{j=-r}^r \mathbf{I}_{\text{CIELab}}^L(x+i, y+j)}{N_B}, \quad (2)$$

$$\begin{aligned} \mathbf{I}_P &= \mathbf{I}_{\text{mean}}(x, y) + 2 \left(\mathbf{I}_{\text{CIELab}}^L(x, y) - \mathbf{I}_{\text{mean}}(x, y) \right) \\ &= \frac{2 \sum_{x=1}^M \sum_{y=1}^N \mathbf{I}_{\text{CIELab}}^L(x, y)}{M \times N} \\ &\quad - \frac{\sum_{i=-r}^r \sum_{j=-r}^r \mathbf{I}_{\text{CIELab}}^L(x+i, y+j)}{N_B}, \end{aligned} \quad (3)$$

where N_B is the sum of pixel points of the local block image and r represents the radius of the window. $\sum_{i=-r}^r \sum_{j=-r}^r \mathbf{I}_{\text{CIELab}}^L(x+i, y+j)$ and $\mathbf{I}_{\text{mean}}(x, y)$ are local image blocks' pixel and mean values. M and N are the height and width of the input image $\mathbf{I}_{\text{CIELab}}^L(x, y)$ and \mathbf{I}_P is the box filtered image.

Subsequently, we evaluate the averages of the a and b channels and update the channel with the smaller pixel average through a color-balancing strategy. This adjustment entails multiplying the ratio of the sum and difference of the two channels' pixel averages by the channel's pixel value with the larger pixel average. Finally, we add the resultant value to the raw channel. When $\bar{\mathbf{I}}_{\text{CIELab}}^a < \bar{\mathbf{I}}_{\text{CIELab}}^b$, this process can be expressed mathematically as

$$\begin{aligned} \mathbf{I}_a^{\text{cc}} &= \mathbf{I}_{\text{CIELab}}^a + \left(\bar{\mathbf{I}}_{\text{CIELab}}^b - \bar{\mathbf{I}}_{\text{CIELab}}^a \right) / \left(\bar{\mathbf{I}}_{\text{CIELab}}^b + \bar{\mathbf{I}}_{\text{CIELab}}^a \right) \\ &\quad \times \mathbf{I}_{\text{CIELab}}^b. \end{aligned} \quad (4)$$

Similarly, when $\bar{\mathbf{I}}_{\text{CIELab}}^a \geq \bar{\mathbf{I}}_{\text{CIELab}}^b$, this process can be expressed mathematically as

$$\begin{aligned} \mathbf{I}_b^{\text{cc}} &= \mathbf{I}_{\text{CIELab}}^b + \left(\bar{\mathbf{I}}_{\text{CIELab}}^a - \bar{\mathbf{I}}_{\text{CIELab}}^b \right) / \left(\bar{\mathbf{I}}_{\text{CIELab}}^a + \bar{\mathbf{I}}_{\text{CIELab}}^b \right) \\ &\quad \times \mathbf{I}_{\text{CIELab}}^a, \end{aligned} \quad (5)$$

where $\bar{\mathbf{I}}_{\text{CIELab}}^a = \sum_{i=1}^M \sum_{j=1}^N \mathbf{I}_{\text{CIELab}}^a(x, y) / (M \times N)$ and $\bar{\mathbf{I}}_{\text{CIELab}}^b = \sum_{i=1}^M \sum_{j=1}^N \mathbf{I}_{\text{CIELab}}^b(x, y) / (M \times N)$ are the pixel averages of the raw image $\mathbf{I}_{\text{CIELab}}^a$ and $\mathbf{I}_{\text{CIELab}}^b$, respectively.

C. Image Decomposition

Inspired by [30], we decompose the color-corrected image into its foreground and background components. Following this decomposition, we apply the percentile maximum-based contrast enhancement method on the foreground image to obtain the foreground contrast-enhanced sub-image. Meanwhile, we utilize the multilayer transmission map estimated dehazing method to obtain the background dehazed sub-image. The decomposition process is represented as

$$k = \frac{\alpha \cdot \mathbf{I}_c^{\text{cc}}(x, y)}{\max(\mathbf{I}_c^{\text{cc}}(x, y))}, \quad x = 1, \dots, M, y = 1, \dots, N, \quad (6)$$

$$\mathbf{I}_F = (1 - k) \times \mathbf{I}_c^{\text{cc}}(x, y), \quad (7)$$

$$\mathbf{I}_B = k \times \mathbf{I}_c^{\text{cc}}(x, y), \quad c \in \{R, G, B\}, \quad (8)$$

where k is the image separation critical value. \mathbf{I}_F and \mathbf{I}_B are the foreground and background images by separated pixel by pixel. In our work, we used $\alpha = 0.5$ as a reference to separate the image.

1) Percentile Maximum-Based Contrast Enhancement:

We perform contrast enhancement on the foreground image based on the percentile maximum-based contrast enhancement method to enhance the image's contrast and texture details. First, traverse the RGB channels of the \mathbf{I}_c^{cc} to update the pixel values in each channel. The pixel values of the pixel points whose image pixel values are less than the first threshold are replaced with the first threshold. In comparison, the pixel values of the pixel points whose pixel values are more significant than the second threshold are replaced with the second threshold. This process is aimed to enhance the contrast of the foreground image, which is represented as

$$(N - 1) \times \alpha = x + y, \quad (9)$$

$$V_1 = (1 - y) \times A[x] + j \times A[x + 1], \quad (10)$$

where $N = \sum_{x=1}^H \sum_{y=1}^W 1$ is the amount of pixels in the image and the height and width are H and W of the foreground image. Meanwhile, α is a percentile, we set it as 0.1%. x and y are the positions of the image pixel point corresponding to the percentile number. V_1 is the threshold corresponding to the percentile and A representative array. The pixel values in the image that are below the threshold V_1 are updated to the threshold V_1 by threshold judgment. It can be articulated as

$$(N - 1) \cdot \beta = x + y, \quad (11)$$

$$V_2 = (1 - y) \times A[x] + y \times A[x + 1], \quad (12)$$

where V_2 is the threshold corresponding to the percentile β , and it is set to $\beta = 99.5\%$ after our experiments and analysis. The pixel values in the image that are greater than the threshold V_2 are updated to the threshold V_2 by threshold judgment. Whereafter, we employ the percentile maximum-based contrast enhancement method to obtain the enhanced image as

$$\mathbf{I}_c^{\text{ce}} = \frac{\mathbf{I}_F^c - \min(\mathbf{I}_F^c(x, y))}{2(\max(\mathbf{I}_F^c(x, y)) - \min(\mathbf{I}_F^c(x, y)))}, \quad (13)$$

where \mathbf{I}_c^{ce} and \mathbf{I}_F^c are the contrast-enhanced image and the pixel value updated foreground image, respectively. Meanwhile, $\min(\mathbf{I}_F^c(x, y))$ and $\max(\mathbf{I}_F^c(x, y))$ are the maximum and minimum values of the foreground image after the updated pixel values.

2) Multilayer Transmission Map Estimated Dehazing: Inspired by conventional dehazing techniques [58], [59], we propose the multilayer transmission map estimated dehazing method. It estimates atmospheric light based on an atmospheric scattering model while using box filtering and moveable window techniques to accurately compute the transmission map based on scene depth similarity assumptions. Ultimately, the image dehazing process merges the estimated atmospheric light with the transmission map.

We present a four-class hierarchical estimation method to estimate atmospheric light, which includes segmenting the background image into four distinct regions and calculating the pixel value, channel pixel means, and standard deviation for each area. The region scoring values are determined using known pixel mean and standard deviation, highlighting the specific content characteristics within each image segment. Subsequently, the areas with the highest scoring values are filtered out, and the iterative process is repeated for these selected areas until the specified range is achieved. The mathematical representation of the atmospheric scattering model as

$$\mathbf{I}_B(x) = \mathbf{J}(x)\mathbf{t}(x) + A(1 - \mathbf{t}(x)), \quad (14)$$

where $\mathbf{I}_B(x)$ and $\mathbf{J}(x)$ are the dehazed and clarified images. $\mathbf{t}(x)$ and A are transmission map and atmospheric light, respectively. The region pixel values are calculated as

$$\begin{aligned} \mathbf{I}_{TL} &= \sum_{x=1}^{M/2} \sum_{y=1}^{N/2} \mathbf{I}_B(x, y), \\ \mathbf{I}_{TR} &= \sum_{x=1}^{M/2} \sum_{y=N/2+1}^{N/2+1} \mathbf{I}_B(x, y), \\ \mathbf{I}_{BL} &= \sum_{x=M/2+1}^{M/2+1} \sum_{y=1}^{N/2} \mathbf{I}_B(x, y), \\ \mathbf{I}_{BR} &= \sum_{x=M/2+1}^{M/2+1} \sum_{y=N/2+1}^{N/2+1} \mathbf{I}_B(x, y), \end{aligned} \quad (15)$$

where \mathbf{I}_{TL} , \mathbf{I}_{TR} , \mathbf{I}_{BL} , and \mathbf{I}_{BR} are the top left, top right, bottom left, and bottom right regions of the background image $\mathbf{I}_B(x, y)$. The process of computing the mean and standard

deviation of the pixel values in the regional image as

$$\bar{\mathbf{I}}^c = \sum_{x=1}^{M/2} \sum_{y=1}^{N/2} \mathbf{I}_B^c(x, y) / \frac{M}{2} \cdot \frac{N}{2}, \quad (16)$$

$$\bar{W}^c = \sqrt{\frac{4}{M \times N} \sum_{x=1}^{M/2} \sum_{y=1}^{N/2} (\mathbf{I}_B^c(x, y) - \bar{\mathbf{I}}^c)^2}, \quad (17)$$

$$P = \sum_{c \in \{R, G, B\}} (\bar{\mathbf{I}}^c - \bar{W}^c), \quad (18)$$

$$\mathbf{I}_{\text{im}} = \max(P_R, P_G, P_B), \quad (19)$$

where $\bar{\mathbf{I}}^c$ and \bar{W}^c are the mean and standard deviation of the background regional image. P represents the pixel rating value and \mathbf{I}_{im} for highest rated area. We compute the Euclidean distance $\|(\mathbf{I}_{\text{im}}^R, \mathbf{I}_{\text{im}}^G, \mathbf{I}_{\text{im}}^B) - (255, 255, 255)\|$ of the pixel from the white pixel in the selected region and choose as bright an atmospheric light as possible by minimizing the distance from the white pixel (255, 255, 255).

Subsequently, the background image is segmented into region blocks based on leveraging the concept of local depth similarity within the scene, each having a size of 15×15 pixels. Transmission maps are estimated for each of these region blocks and these individual maps are subsequently merged to yield the transmission map for the entire image to effectively restore concealed information in underwater images and enhance overall image quality. The Eq. (14) can be rewritten from the above solution as

$$\mathbf{J}(x) = \frac{\mathbf{I}_B(x) - A(1 - \mathbf{t}(x))}{\mathbf{t}(x)}. \quad (20)$$

From the above Eq. (20), we know the recovery of the background image after estimating the A depends on $\mathbf{t}(x)$ and the contrast of the recovered image increases as $\mathbf{t}(x)$ decreases, which leads to finding the optimal $\mathbf{t}(x)$ so that the recovered image has the maximum contrast. The optimal estimation is calculated as

$$\mathbf{J}^c = A^c + \frac{(\mathbf{I}_B^c - A^c)T}{128}, \quad (21)$$

$$E = \sum_{c \in \{R, G, B\}} \sum_{k \in B} \left\{ (\min\{0, \mathbf{J}^c(k)\})^2 + (\max\{0, \mathbf{J}^c(k) - 255\})^2 \right\}, \quad (22)$$

$$\begin{aligned} \text{FC} &= \frac{\lambda E}{N_B} - \left(\frac{\sum_{c \in \{R, G, B\}} \sum_{k \in B} (\mathbf{J}^c(k))^2}{N_B} \right. \\ &\quad \left. - \left(\frac{\sum_{c \in \{R, G, B\}} \sum_{k \in B} (\mathbf{J}^c(k))}{N_B} \right)^2 \right), \end{aligned} \quad (23)$$

where \mathbf{J}^c and \mathbf{I}_B^c are the clarified and background image. T and E are the initial transmission map and loss of dehazing process. FC is the cost function assessing the quality of the dehazed image concerning the iteratively updated current transmission map. λ represents the parameter controlling the balance between information loss and mean deviation. N_B is

the total number of pixel points in the background image block. In which $\frac{\sum_{c \in \{R, G, B\}} \sum_{k \in B} (J^c(k))^2}{N_B}$ and $\frac{\sum_{c \in \{R, G, B\}} \sum_{k \in B} (J^c(k))}{N_B}$ are employed to evaluate the image's contrast and brightness.

In the iterative process, we calculate the cost function associated with different transmission maps to determine the most effective dehazing option. However, it's important to note that variations in real-world scene depth among different image blocks can lead to artifacts within the images. To address this challenge, we propose the transmission maps optimization of the image blocks using guided filtering. This enhancement ensures that the transmission mapped closely corresponds to the depth variations in the actual scene, thereby reducing artifacts and preserving image details. After obtaining atmospheric light and transmission map, the dehazing process can be expressed as

$$\mathbf{I}_{\text{Max}} = \max \left(\frac{\sum_{x=1}^M \sum_{y=1}^N \mathbf{I}_B^c(x, y)}{M \times N} \right), c \in \{R, G, B\}, \quad (24)$$

$$\mathbf{I}_Y^c = \frac{\mathbf{I}_{\text{Max}}}{\sum_{x=1}^M \sum_{y=1}^N \mathbf{I}_B^c(x, y) / (M \times N)}, \quad (25)$$

$$\mathbf{T}^c = \mathbf{T}^{\beta \cdot \mathbf{I}_Y^c}, \quad (26)$$

$$\mathbf{J}(x) = (\mathbf{I}_N - A_N) \mathbf{T}^c + A_N, N = 1, 2, 3, \quad (27)$$

where \mathbf{I}_{Max} is the largest average pixel value in the background image $\mathbf{I}_B^c(x, y)$. \mathbf{I}_Y^c is the ratio of the maximum channel pixel average to the channel pixel mean in the background image. \mathbf{T} and \mathbf{T}^c are the optimized and gain-adjusted transmission maps.

D. Principal Component Analysis Fusion

Unlike previous fusion methods [61], [62], [63], we employ a principal component analysis fusion strategy to obtain a clarified underwater image by integrating the advantage features of the foreground contrast-enhanced and the background dehazed sub-images. The fusion weights are determined by analyzing the eigenvalues and eigenvectors of the covariance matrices of the foreground and background images. Subsequently, the foreground and background images are linearly combined based on these weights to produce the fused image. This approach effectively retains the raw image's texture details and improves image quality. We first compute the covariance matrix of the foreground contrast-enhanced and the background dehazed images. The process of solving the covariance matrix is defined as

$$\mathbf{I}_{\text{CM}} = \text{Con}(\mathbf{I}_F, \mathbf{I}_B) = \frac{\sum_{i=1}^n (\mathbf{I}_{F^i} - \bar{\mathbf{I}}_F)(\mathbf{I}_{B^i} - \bar{\mathbf{I}}_B)}{n - 1}, n = 3, \quad (28)$$

where \mathbf{I}_F and \mathbf{I}_B are the foreground enhanced image and the background dehazed image, respectively. \mathbf{I}_{CM} is the covariance matrix, $\bar{\mathbf{I}}_F$ and $\bar{\mathbf{I}}_B$ are the image pixel averages.

Specifically, we utilize the $f_{\text{eig}}(\cdot)$ function to solve the eigenvalues λ and eigenvectors α of the matrix based on the calculated covariance matrix, in which the eigenvalues signify the magnitude of variance within the covariance matrix to assess the information associated with the principal component directions. Then, select the eigenvectors corresponding to larger feature values and divide them by the sum of the feature values to obtain the normalized weights. Utilize these normalized weights to generate the ultimate enhanced result. The mathematical expression of the normalized weight as

$$\omega_1 = \frac{\alpha 1}{\sum_{i=1}^M \alpha_i}, \omega_2 = \frac{\alpha 2}{\sum_{i=1}^M \alpha_i}, \alpha 1 > \alpha 2, \quad (29)$$

$$\omega_1 = \frac{\alpha 2}{\sum_{i=1}^M \alpha_i}, \omega_2 = \frac{\alpha 1}{\sum_{i=1}^M \alpha_i}, \alpha 1 > \alpha 2, \quad (30)$$

where ω_1 and ω_2 are the normalized weights. The final fusion is defined as

$$\mathbf{Z}(x) = 2\omega_1 \times \mathbf{I}_F(x) + 2\omega_2 \times \mathbf{I}_B(x), \quad (31)$$

where ω_1 and ω_2 are the normalized weights. $\mathbf{Z}(x)$, $\mathbf{I}_F(x)$, and $\mathbf{I}_B(x)$ are the final enhanced image, foreground contrast-enhanced image, and background dehazed image, respectively.

IV. EXPERIMENTS AND DISCUSSIONS

In this section, we conduct comprehensive quantitative and qualitative evaluations of our proposed PCFB method on three standard datasets [64], [65]. Additionally, we analyze the results of the ablation study, explore various applications, and conduct extended experiments to prove the robust performance of our PCFB. Due to space constraints, some results are presented in the supplementary material.

Compared Methods: Our PCFB method is compared with 12 methods, including IBLA [55], GDCP [13], GIFM [16], ULAP [19], WCBF [49], HFM [44], LANet [52], WaterNet [32], PUIE-Net [60], UIEC-Net [35], SGUIE-Net [36], and CLUIE-Net [39].

Benchmark Datasets: Our PCFB is implemented on three datasets UCCS [40], UIQS [40], and UIEB [32]. The UCCS [40] dataset contains three color subsets, which are used to validate the color correction ability of the enhancement method. The UIQS [40] contains five subsets of 726 images each, validating enhancement methods' visibility performance. The UIEB [32] dataset contains different scenes and degradation levels of underwater images, which is employed to evaluate the generalization performance of different methods.

Evaluation Metrics: We utilize four widely adopted image quality evaluation metrics to evaluate the enhancement performance of various methods quantitatively, and they include edge intensity (EI) [66], average gradient (AG) [30], information entropy (IE) [67], and colorfulness contrast fog density index (CCF) [68]. In comparison, a higher value of EI [66] represents a more pronounced delineation of edges in the enhanced image, AG [30] signifies improved visibility in the enhanced image, and a higher value of IE [67] indicates enhanced detail. Additionally, a higher CCF [68] value signifies an enhanced visual perception of the improved image.

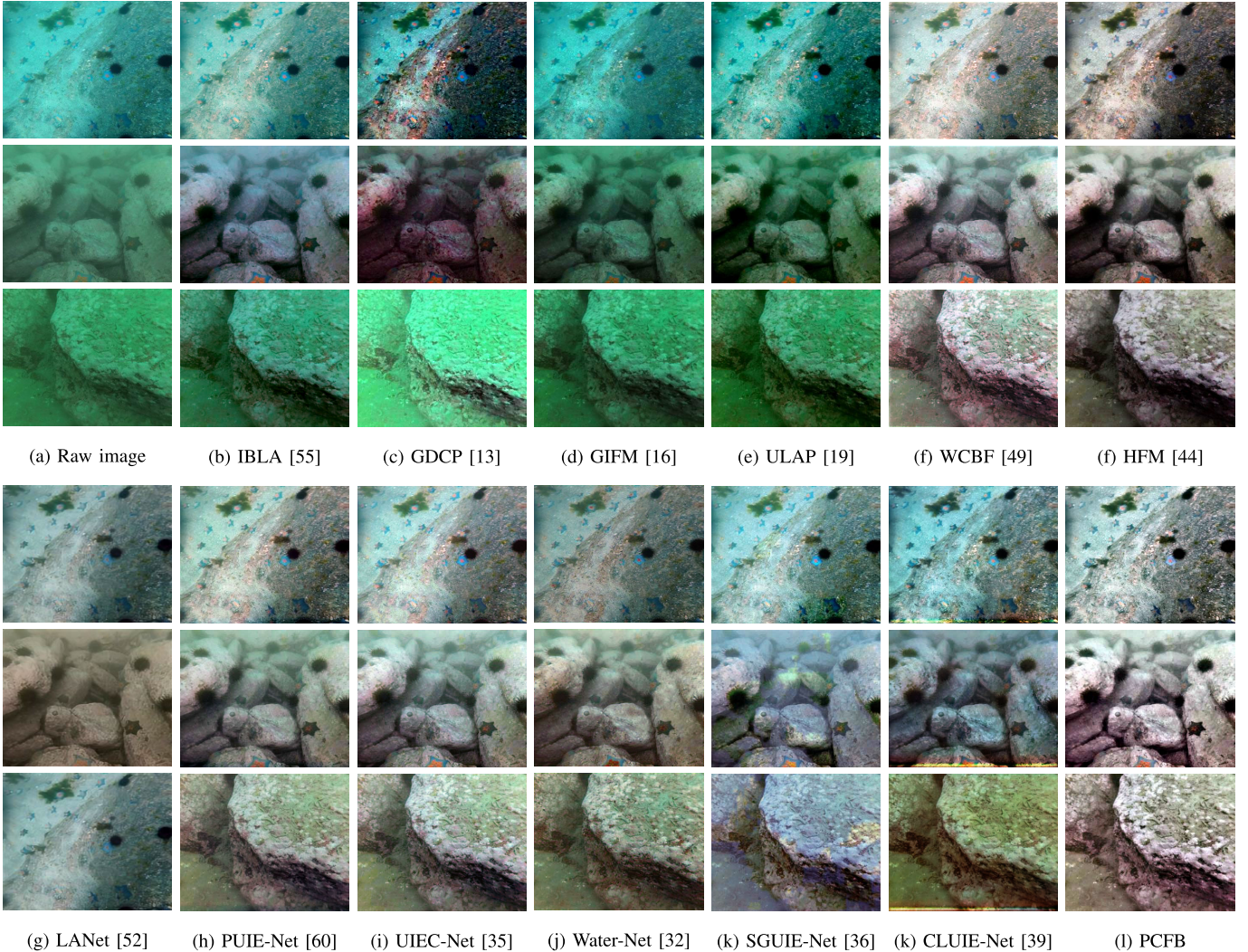


Fig. 3. The enhancement result on the UCCS [40] dataset. The Raw is low quality underwater images sampled from the UCCS [40]. The others are clarified underwater images processed by different enhancement methods.

A. Evaluation on the UCCS

1) *Qualitative Comparisons:* We performed a comparative analysis to assess the color correction performance of our PCFB in comparison to ten other enhancement methods on the UCCS dataset [40]. From Fig. 3, these images represent three random samples taken from blue, blue-green, and green subsets, respectively. IBLA [55], GDCP [13], GIFM [16], and ULAP [19] obtain unsatisfactory color correction performance on the blue and green subsets, whereas IBLA [55] and GDCP [13] introduce purple and dark red artifacts when restoring blue subsets images. The application of methods WCBF [49], HFM [44], LANet [52], SGUIE-Net [36], and CLUIE-Net [39] significantly improve the image's contrast and texture but introduce undesirable color distortions, including reddish, yellow, and purple artifacts. In contrast, PUIE-Net [60], UIEC-Net [35], and Water-Net [32] have good color correction capabilities on underwater images but exhibit blurriness in the enhanced image. In comparison, it is clear that our method excels in rectifying color bias, enhancing contrast, and refining texture details in the images.

2) *Quantitative Comparisons:* Table I presents the EI [66], AG [30], IE [67], and CCF [68] scores obtained by various methods in experiments conducted on the UCCS dataset [40]. The results indicate that our PCFB achieves the highest or nearly the highest scores on the blue-green and green subsets, and our PCFB has the highest or almost the highest scores in addition to the IE [67] index on the blue subset, which proves that our PCFB effectively rectifies color biases while enhancing texture details and contrast across the three subsets. In conclusion, our method demonstrates favorable qualitative and quantitative outcomes on the UCCS dataset [40].

B. Evaluation on the UIQS

1) *Qualitative Comparisons:* We compared the visible performance of our PCFB and ten other enhancement methods on the UIQS [40] dataset. From Fig. 4, GDCP [13], GIFM [16], and ULAP [19] failed to address color deviations of the B, C, D, and E subsets. In addition, GDCP [13] and ULAP [19] appear as local overexposure phenomena, and GIFM [16] recovery results show local color distortion and overall

TABLE I

QUANTITATIVE EVALUATION OF THE METRICS VALUES FOR VARIOUS METHODS ASSESSED ON THE UCCS [40]. THE HIGHEST QUANTITATIVE SCORES ARE MARKED IN RED, AND THE NEXT HIGHEST SCORES ARE REPRESENTED IN BLUE

Methods	Blue				Blue-green				Green			
	EI ↑	AG ↑	IE ↑	CCF ↑	EI ↑	AG ↑	IE ↑	CCF ↑	EI ↑	AG ↑	IE ↑	CCF ↑
IBLA [55]	72.286	7.519	7.484	35.158	30.520	2.934	7.204	17.685	30.033	2.900	6.944	24.994
GDCP [13]	92.879	9.679	7.442	37.725	39.270	3.791	7.169	17.304	34.497	3.342	6.861	19.434
GIFM [16]	51.998	5.383	7.551	27.067	31.594	3.029	7.478	26.212	24.381	2.336	7.003	17.594
ULAP [19]	75.251	7.869	7.473	44.511	32.896	3.156	7.823	25.096	25.142	2.419	6.909	25.418
WCBF [49]	84.911	8.917	7.623	21.965	52.573	5.135	7.637	20.051	57.523	5.646	7.635	20.230
HFM [44]	94.946	9.904	7.805	34.031	54.067	5.162	7.802	33.043	50.429	4.827	7.773	31.654
LANet [52]	51.970	5.098	7.306	20.780	36.285	3.501	7.019	15.855	33.211	3.214	7.031	19.548
Water-Net [32]	61.914	6.424	7.183	17.339	40.521	3.903	7.408	17.020	43.778	4.205	7.392	17.413
PUIE-Net [60]	73.274	7.571	7.556	24.075	38.910	3.716	7.391	17.866	36.150	3.453	7.271	16.740
UIEC-Net [35]	80.703	8.398	7.674	21.920	45.001	4.364	7.557	18.790	44.708	4.360	7.526	18.418
SGUIE-Net [36]	81.947	8.538	7.700	29.430	46.126	4.416	7.559	20.321	41.582	3.968	7.525	21.367
CLUIE-Net [39]	91.880	9.564	7.696	24.378	45.589	4.376	7.380	17.614	31.674	3.036	7.051	14.690
PCFB	111.787	11.647	7.691	37.134	68.158	6.504	7.677	32.334	66.047	6.291	7.676	33.722

darkness of the A subset. IBLA [55] introduces an additional purplish tone of the B and D subsets. SGUIE-Net [47] and CLUIE-Net [39] improve contrast and texture details that are significant in images but that introduce an additional yellowish and mauve tone. LANet [52], Water-Net [32], UIEC-Net [35], and PUIE-Net [60] effectively correct the color deviation while enhancing the contrast of the image, but the enhancement result has local color distortion and undersaturation. WCBF [49] and HFM [44] enhance brightness, contrast, and saturation, but they fall short of improving structural detail. In contrast, the approach successfully corrects color deviations, accentuates details, and heightens visibility without inducing excessive enhancement or oversaturation. Additional visual results and corresponding histogram distributions are available in our supplementary material, affirming the robustness and generalizability of our method in the datasets.

2) *Quantitative Comparisons*: Table II presents the IE [67], AG [30], EI [66], and CCF [68] scores for various methods evaluated on the UIQS [40] dataset. It is evident that our PCFB outperformed other methods from Table II, our method achieves the highest value or near the highest value except for the IE [67] value in subset A. In general, our PCFB exhibits superior results compared to the alternative methods in assessments of underwater images across all five subsets.

C. Evaluation on the UIEB

1) *Qualitative Comparisons*: For a more comprehensive assessment of our PCFB method's performance across diverse underwater scenes and degradation types, we randomly selected several underwater images from the UIEB [32] dataset. We quantitatively compared our PCFB with other existing methods. More visual results and the corresponding histogram distribution in the supplementary material. In Fig. 5, IBLA [55], GDCP [13], GIFM [16], and ULAP [19] fail to effectively enhance the visibility and unable to correct color biases of low-visibility underwater images. Relatively, LANet [52] improves image contrast and sharpness but introduces unwanted yellow and cyan tones. SGUIE-Net [36] and CLUIE-Net [39] effectively correct image color shifts when

enhancing blue images, but localized overexposure occurs, and violet tones are introduced when enhancing blurred and green images. Additionally, WCBF [49], HFM [44], Water-Net [32], UIEC-Net [35], and PUIE-Net [60] successfully address color biases in low-visibility images, they struggle to enhance contrast and may encounter issues of local darkness and underenhancement. Water-Net [32] introduces local darkness in certain scenarios. In contrast, our PCFB adeptly eliminates unnatural colors, enhances visibility, and improves clear visual images.

2) *Quantitative Comparisons*: Table III presents the IE [67], AG [30], EI [66], and CCF [68] scores for various methods evaluated on the UIEB [32] dataset. The outcomes demonstrate our PCFB method outperformed others, except for the IE value. Overall, our PCFB demonstrates good performance across the three standard datasets.

D. Ablation Study

To illustrate the individual contributions of each core part in our PCFB to results, we conducted ablation analyses on the three datasets, including (a) our PCFB without color balance-guided color correction (-w/o CBCC); (b) our PCFB without foreground contrast-enhanced (-w/o FCES); (c) our PCFB without background dehazed (-w/o BDSI); (d) our PCFB without principal component analysis fusion (-w/o PCAF). Fig. 6 displays the results of our PCFB on the three datasets.

The results depicted in Fig. 6 can be summarized as (a) -w/o CBCC unable to color correct underwater images; (b) -w/o FCES underwater images were color corrected, but purple artifacts were introduced and over-enhancement problems existed; (c) -w/o BDSI improves the image color, but the enhanced image is overall blurrier and less contrasty; (d) -w/o PCAF effectively improves image color and texture details, but the image is darker overall, and All parts of the complete composition of the enhanced underwater map under the better results achieved, in terms of clarity, texture details, contrast, color have a better performance.

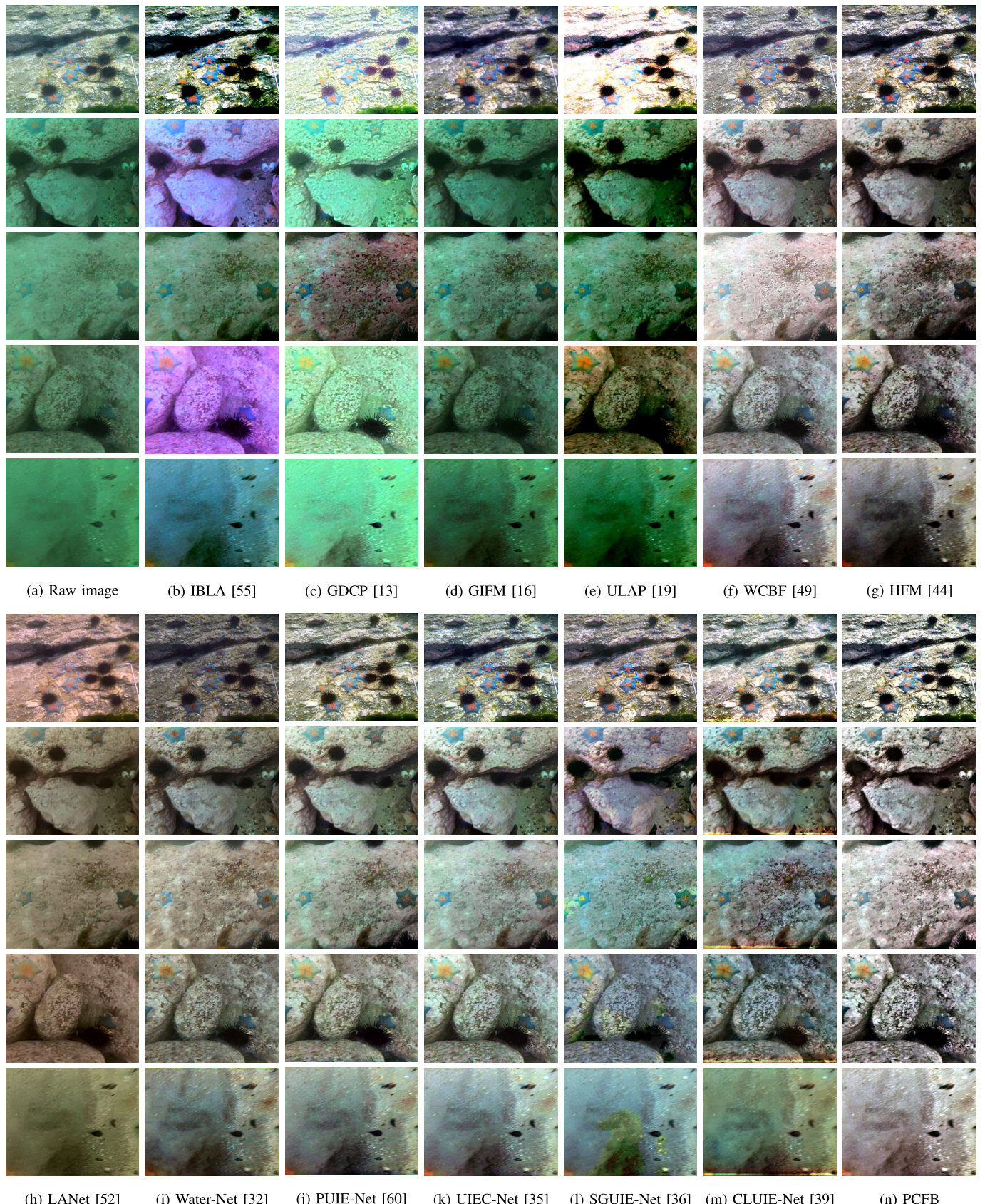


Fig. 4. **The enhancement result on the UIQS dataset [40].** The Raw is low quality underwater image form the UIQS [40]. The others are enhancement result images and corresponding RGB distribution histograms processed by different image enhancement methods.

TABLE II
QUANTITATIVE EVALUATION OF THE METRICS VALUES FOR VARIOUS METHODS ASSESSED ON THE UIQS [40]

Metric	IBLA [55]	GDCP [13]	GIFM [16]	ULAP [19]	WCBF [49]	HFM [44]	LANet [52]	Water-Net [32]	PUIE-Net [60]	UIEC-Net [35]	SGUIE-Net [36]	CLUIE-Net [39]	PCFB
A	EI↑ 84.705	97.978	70.516	93.390	87.152	106.463	62.814	65.151	85.122	92.277	92.037	104.496	130.750
	AG↑ 8.644	10.057	6.707	9.627	8.907	10.898	6.133	6.654	8.622	9.397	9.335	10.654	13.265
	IE↑ 7.360	7.417	7.626	7.631	7.145	7.797	7.418	7.132	7.651	7.717	7.661	7.704	7.673
B	CCF↑ 40.845	31.654	28.351	24.695	48.347	37.737	30.598	18.687	28.629	25.673	31.791	30.323	46.482
	EI↑ 53.435	65.855	44.004	74.623	54.658	76.010	48.028	55.588	59.679	68.444	66.744	67.964	96.533
	AG↑ 5.220	6.456	4.277	7.367	5.333	7.394	4.657	5.439	5.784	6.703	6.499	6.610	9.361
C	IE↑ 7.284	7.287	7.325	7.616	7.128	7.734	7.163	7.285	7.466	7.610	7.541	7.457	7.697
	CCF↑ 27.781	23.147	21.592	22.468	35.621	33.992	22.249	18.580	22.381	22.253	25.935	22.749	37.343
	EI↑ 45.361	55.728	37.561	67.661	44.455	67.119	43.630	50.26	51.873	60.196	58.860	56.597	86.426
D	AG↑ 4.413	5.440	3.637	6.662	4.320	6.494	4.232	4.895	5.001	5.881	5.700	5.482	8.341
	IE↑ 7.216	7.179	7.269	7.601	7.036	7.731	7.105	7.298	7.402	7.569	7.509	7.341	7.669
	CCF↑ 25.137	21.435	20.743	21.102	31.879	33.042	20.551	17.528	20.209	20.484	23.403	19.871	36.271
E	EI↑ 29.487	34.587	25.779	51.850	27.682	49.321	34.045	38.984	35.690	42.003	40.428	36.322	62.895
	AG↑ 2.857	3.363	2.479	5.103	2.676	4.736	3.301	3.771	3.428	4.102	3.885	3.500	6.027
	IE↑ 7.110	6.897	7.269	7.582	7.047	7.767	7.043	7.325	7.295	7.489	7.458	7.171	7.616
CCF↑ 19.776	16.623	20.676	18.018	23.615	30.010	18.300	15.197	15.920	16.712	18.936	14.824	31.418	
	EI↑ 30.294	34.286	26.092	49.192	28.924	28.617	32.820	36.089	35.004	40.709	38.953	37.215	61.211
	AG↑ 2.940	3.339	2.516	4.853	2.800	4.557	3.184	3.505	3.371	3.982	3.756	3.594	5.888
CCF↑ 7.206	6.944	7.339	7.552	7.103	7.757	7.079	7.283	7.301	7.501	7.432	7.238	7.604	
	19.711	16.168	21.959	17.146	25.472	28.617	17.368	14.133	15.467	16.018	18.003	14.903	31.265

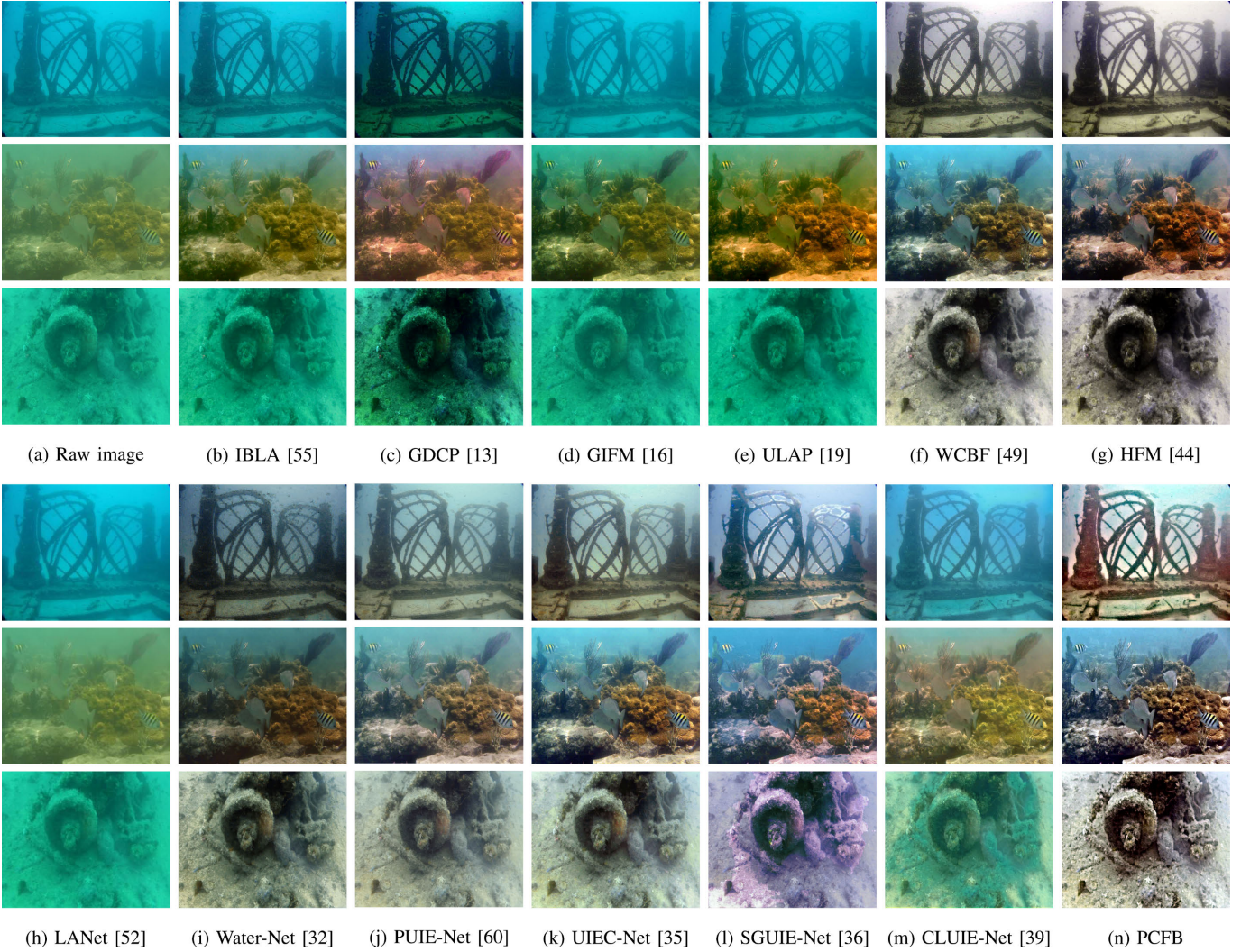


Fig. 5. The enhancement result on the UIEB [32] dataset. Raw are low quality underwater images sampled from the UIEB [32], respectively. The others are clarified underwater images processed by different enhancement methods.

Table IV showcases the IE [67], AG [30], EI [66], and CCF [68] scores corresponding to each core part of our PCFB is evaluated on the three datasets. Table IV illustrates that our full model consistently attains optimal or near-optimal scores across various metrics. The ablation study highlights each core part's positive influence on the ultimate enhancement outcome.

E. Applications

To prove the effectiveness of our PCFB, we test the application of our PCFB on underwater image color segmentation and critical point detection as shown in Fig. 7.

1) *Color Segmentation*: We employ a fast fuzzy C-means (FCM) clustering method based on superpixels for the

TABLE III
QUANTITATIVE EVALUATION OF THE METRICS VALUES FOR VARIOUS METHODS ASSESSED ON THE UIEB [32] DATASET

Metric	IBLA [55]	GDCP [13]	GIFM [16]	ULAP [19]	WCBF [49]	HFM [44]	LANet [52]	Water-Net [32]	PUIE-Net [60]	UIEC-Net [35]	SGUIE-Net [36]	CLUIE-Net [39]	PCFB
EI↑	62.321	73.994	50.635	64.637	63.534	72.009	77.405	43.054	60.041	66.295	74.102	74.390	100.193
AG↑	6.308	7.526	5.118	6.611	6.410	7.260	7.760	4.327	6.004	6.692	7.451	7.507	10.105
IE↑	7.282	7.302	7.425	7.546	7.186	7.739	7.670	7.005	7.584	7.689	7.669	7.625	7.569
CCF↑	38.365	33.211	26.621	19.878	39.625	34.247	31.850	15.281	21.596	20.827	31.662	23.599	44.770

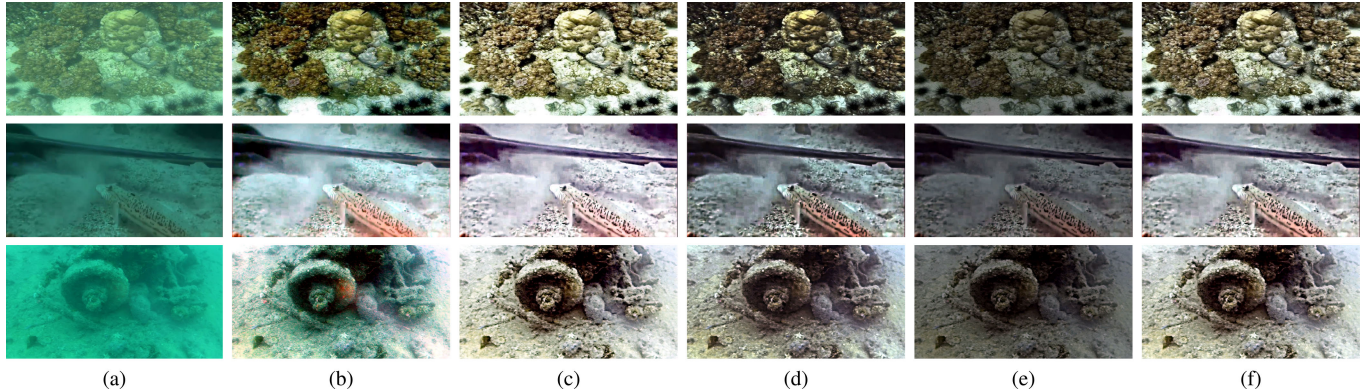


Fig. 6. Ablation results for each part component of our method. The (a) are low quality underwater images from the three datasets. (b) -w/o CBCC. (c) -w/o FCES. (d) -w/o BDSI. (e) -w/o PCAF. (f) PCFB.

TABLE IV
ABLATION STUDIES ARE CONDUCTED ON THE THREE DATASETS

Methods	UCCS [40]				UIQS [40]				UIEB [32]			
	EI↑	AG↑	IE↑	CCF↑	EI↑	AG↑	IE↑	CCF↑	EI↑	AG↑	IE↑	CCF↑
-w/o CBCC	66.252	6.675	7.729	34.348	70.548	6.908	7.702	36.329	75.184	7.582	7.481	45.069
-w/o FCES	67.913	6.578	7.041	33.567	73.137	7.082	6.911	35.589	88.638	8.983	6.254	40.274
-w/o BDSI	64.164	6.264	7.294	26.878	66.422	6.475	7.121	27.807	75.352	7.682	6.146	31.276
-w/o PCAF	26.357	2.658	7.127	12.753	42.409	4.161	6.850	21.828	49.041	4.941	6.670	30.161
PCFB (full model)	81.998	8.114	7.681	34.397	87.563	8.576	7.652	36.556	100.193	10.105	7.569	44.770

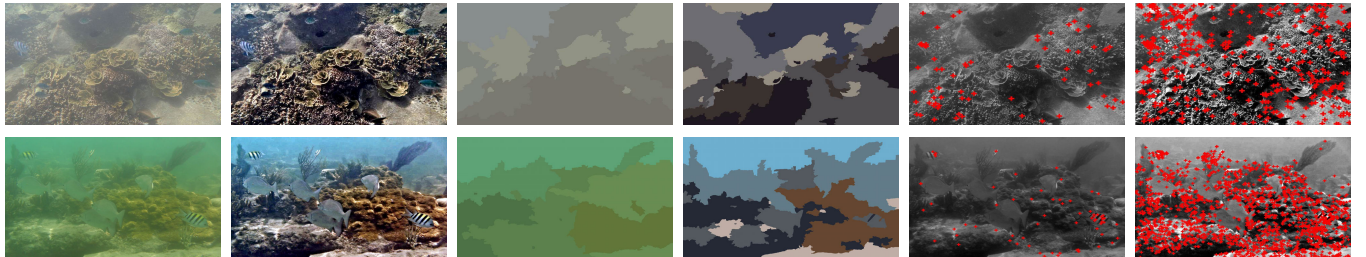


Fig. 7. Application of color segmentation and keypoint detection in underwater images. From left to right, it presents the raw images, images enhanced by our PCFB, and the comparative application of raw images alongside their enhanced versions.

color segmentation of underwater images. By utilizing fuzzy C-means clustering to extract color features from the image and categorizing superpixels into different color classes, this method can offer more precise color segmentation information for practical applications. As depicted in Fig. 7, the image segmentation results processed by our PCFB show greater consistency.

2) *Keypoint Detection:* We employ the SIFT algorithm to compute keypoints in both the raw and enhanced underwater images, as illustrated in Fig. 7. The raw low-quality underwater image exhibits 72 and 69 keypoints, while the underwater image enhanced using our method displays 409 and 1714 keypoints. This demonstrates a substantial rise in the number of

detected keypoints detected in the image enhanced through our PCFB method.

F. Extended Experiment

Our proposed PCFB method for underwater image enhancement demonstrates superior performance in enhancing underwater images and in its applicability to haze and low-light images. From Fig. 8, the top segment of Fig. 8 (a) depicts a dehazed image, followed by an image enhanced using our method, showcasing a significant improvement in contrast and clarity. In Fig. 8 (b), the upper segment represents a low-light image, succeeded by an image enhanced by our method, demonstrating superior color vividness and enhanced texture



Fig. 8. Displayed here are the enhancement outcomes of our PCFB for dehazing and low-light images. The top row exhibits the original low-quality images, while the bottom row showcases the images enhanced by our PCFB.

details. Notably, these enhancements were achieved without parameter fine-tuning, reinforcing the remarkable generalization performance of our PCFB.

V. CONCLUSION

In our underwater visual clarity task, we designed a principal component fusion method of foreground and background to solve the underwater vision issue. Our PCFB fully exploits the advantageous features of hazed and contrast-enhanced images to obtain clear underwater images. We introduce the percentile maximum-based contrast enhancement method and the multilayer transmission map estimated dehazing method of the color-corrected image to obtain the contrast-enhanced foreground and dehazed background images. We utilize principal component analysis fusion to combine advantageous features of the contrast-enhanced image and the dehazed image to get high-quality underwater images. Extensive experiments on diverse benchmarks have showcased the efficacy and resilience of our PCFB. Additionally, our PCFB method proves advantageous for numerous underwater vision tasks and exhibits strong generalization capabilities for enhancing dehazing and low-light images.

Compared with most existing methods, although our approach has achieved satisfactory results in most cases, it has some limitations. Specifically, when processing images with blue color distortion, our method may introduce unnecessary redness in local edge areas, which is one of the issues to address in future work.

REFERENCES

- [1] Q. Qi et al., "Underwater image co-enhancement with correlation feature matching and joint learning," *IEEE Trans. Circuits Syst. Video Technol.*, vol. 32, no. 3, pp. 1133–1147, Mar. 2022.
- [2] H. Wang, S. Sun, and P. Ren, "Meta underwater camera: A smart protocol for underwater image enhancement," *ISPRS J. Photogramm. Remote Sens.*, vol. 195, pp. 462–481, Jan. 2023.
- [3] L. Chen et al., "Perceptual underwater image enhancement with deep learning and physical priors," *IEEE Trans. Circuits Syst. Video Technol.*, vol. 31, no. 8, pp. 3078–3092, Aug. 2021.
- [4] Q. Jiang, Y. Gu, C. Li, R. Cong, and F. Shao, "Underwater image enhancement quality evaluation: Benchmark dataset and objective metric," *IEEE Trans. Circuits Syst. Video Technol.*, vol. 32, no. 9, pp. 5959–5974, Sep. 2022.
- [5] J. Zhou et al., "UGIF-Net: An efficient fully guided information flow network for underwater image enhancement," *IEEE Trans. Geosci. Remote Sens.*, vol. 61, 2023, Art. no. 4206117.
- [6] C. Li, S. Anwar, J. Hou, R. Cong, C. Guo, and W. Ren, "Underwater image enhancement via medium transmission-guided multi-color space embedding," *IEEE Trans. Image Process.*, vol. 30, pp. 4985–5000, 2021.
- [7] B. McGlamery, "A computer model for underwater camera systems," *Proc. SPIE*, vol. 208, pp. 221–231, Mar. 1980.
- [8] J. S. Jaffe, "Computer modeling and the design of optimal underwater imaging systems," *IEEE J. Ocean. Eng.*, vol. 15, no. 2, pp. 101–111, Apr. 1990.
- [9] Z. Liang, X. Ding, Y. Wang, X. Yan, and X. Fu, "GUDCP: Generalization of underwater dark channel prior for underwater image restoration," *IEEE Trans. Circuits Syst. Video Technol.*, vol. 32, no. 7, pp. 4879–4884, Jul. 2022.
- [10] J. Wang et al., "Periodic integration-based polarization differential imaging for underwater image restoration," *Opt. Lasers Eng.*, vol. 149, Feb. 2022, Art. no. 106785.
- [11] Y. Li, R. Ruan, Z. Mi, X. Shen, T. Gao, and X. Fu, "An underwater image restoration based on global polarization effects of underwater scene," *Opt. Lasers Eng.*, vol. 165, Jun. 2023, Art. no. 107550.
- [12] K. He, J. Sun, and X. Tang, "Single image haze removal using dark channel prior," *IEEE Trans. Pattern Anal. Mach. Intell.*, vol. 33, no. 12, pp. 2341–2353, Dec. 2011.
- [13] Y. Peng, K. Cao, and P. C. Cosman, "Generalization of the dark channel prior for single image restoration," *IEEE Trans. Image Process.*, vol. 27, no. 6, pp. 2856–2868, Jun. 2018.
- [14] J. Li, Q. Hu, and M. Ai, "Haze and thin cloud removal via sphere model improved dark channel prior," *IEEE Geosci. Remote Sens. Lett.*, vol. 16, no. 3, pp. 472–476, Mar. 2019.
- [15] S. C. Agrawal and A. S. Jalal, "A comprehensive review on analysis and implementation of recent image dehazing methods," *Arch. Comput. Methods Eng.*, vol. 29, no. 7, pp. 4799–4850, Nov. 2022.
- [16] Z. Liang, W. Zhang, R. Ruan, P. Zhuang, and C. Li, "GIFM: An image restoration method with generalized image formation model for poor visible conditions," *IEEE Trans. Geosci. Remote Sens.*, vol. 60, 2022, Art. no. 4110616.
- [17] Z. Liang, R. Ruan, L. Jiao, W. Zhang, and P. Zhuang, "An underwater image restoration method based on adaptive brightness improvement and local image descattering," *IEEE Geosci. Remote Sens. Lett.*, vol. 20, pp. 1–5, 2023.
- [18] J. Xie, G. Hou, G. Wang, and Z. Pan, "A variational framework for underwater image dehazing and deblurring," *IEEE Trans. Circuits Syst. Video Technol.*, vol. 32, no. 6, pp. 3514–3526, Jun. 2022.
- [19] J. Li, G. Hou, and G. Wang, "Underwater image restoration using oblique gradient operator and light attenuation prior," *Multimedia Tools Appl.*, vol. 82, no. 5, pp. 6625–6645, Feb. 2023.
- [20] X. Li, G. Hou, K. Li, and Z. Pan, "Enhancing underwater image via adaptive color and contrast enhancement, and denoising," *Eng. Appl. Artif. Intell.*, vol. 111, May 2022, Art. no. 104759.
- [21] W. Zhang, L. Dong, T. Zhang, and W. Xu, "Enhancing underwater image via color correction and bi-interval contrast enhancement," *Signal Process., Image Commun.*, vol. 90, Jan. 2021, Art. no. 116030.
- [22] N. Singh and A. K. Bhandari, "Noise aware L2–LP decomposition-based enhancement in extremely low light conditions with Web application," *IEEE Trans. Consum. Electron.*, vol. 68, no. 2, pp. 161–169, May 2022.
- [23] S. Sharma and T. Varma, "Graph signal processing based underwater image enhancement techniques," *Eng. Sci. Technol., Int. J.*, vol. 32, Aug. 2022, Art. no. 101059.
- [24] W. Zhang, Y. Wang, and C. Li, "Underwater image enhancement by attenuated color channel correction and detail preserved contrast enhancement," *IEEE J. Ocean. Eng.*, vol. 47, no. 3, pp. 718–735, Jul. 2022.
- [25] C.-Y. Li, J.-C. Guo, R.-M. Cong, Y.-W. Pang, and B. Wang, "Underwater image enhancement by dehazing with minimum information loss and histogram distribution prior," *IEEE Trans. Image Process.*, vol. 25, no. 12, pp. 5664–5677, Dec. 2016.

- [26] W. Zhang, L. Dong, and W. Xu, "Retinex-inspired color correction and detail preserved fusion for underwater image enhancement," *Comput. Electron. Agricul.*, vol. 192, Jan. 2022, Art. no. 106585.
- [27] P. Zhuang, C. Li, and J. Wu, "Bayesian retinex underwater image enhancement," *Eng. Appl. Artif. Intell.*, vol. 101, May 2021, Art. no. 104171.
- [28] P. Zhuang, J. Wu, F. Porikli, and C. Li, "Underwater image enhancement with hyper-Laplacian reflectance priors," *IEEE Trans. Image Process.*, vol. 31, pp. 5442–5455, 2022.
- [29] W. Zhang, S. Jin, P. Zhuang, Z. Liang, and C. Li, "Underwater image enhancement via piecewise color correction and dual prior optimized contrast enhancement," *IEEE Signal Process. Lett.*, vol. 30, pp. 229–233, 2023.
- [30] W. Zhang, P. Zhuang, H.-H. Sun, G. Li, S. Kwong, and C. Li, "Underwater image enhancement via minimal color loss and locally adaptive contrast enhancement," *IEEE Trans. Image Process.*, vol. 31, pp. 3997–4010, 2022.
- [31] F. Gao, K. Wang, Z. Yang, Y. Wang, and Q. Zhang, "Underwater image enhancement based on local contrast correction and multi-scale fusion," *J. Mar. Sci. Eng.*, vol. 9, no. 2, p. 225, Feb. 2021.
- [32] C. Li et al., "An underwater image enhancement benchmark dataset and beyond," *IEEE Trans. Image Process.*, vol. 29, pp. 4376–4389, 2020.
- [33] C. Li, S. Anwar, and F. Porikli, "Underwater scene prior inspired deep underwater image and video enhancement," *Pattern Recognit.*, vol. 98, Feb. 2020, Art. no. 107038.
- [34] N. Jiang, W. Chen, Y. Lin, T. Zhao, and C.-W. Lin, "Underwater image enhancement with lightweight cascaded network," *IEEE Trans. Multimedia*, vol. 24, pp. 4301–4313, 2022.
- [35] Y. Wang, J. Guo, H. Gao, and H. Yue, "UIEC²-Net: CNN-based underwater image enhancement using two color space," *Signal Process., Image Commun.*, vol. 96, 2021, Art. no. 116250.
- [36] Q. Qi, K. Li, H. Zheng, X. Gao, G. Hou, and K. Sun, "SGUIE-Net: Semantic attention guided underwater image enhancement with multi-scale perception," *IEEE Trans. Image Process.*, vol. 31, pp. 6816–6830, 2022.
- [37] R. Cong et al., "PUGAN: Physical model-guided underwater image enhancement using GAN with dual-discriminators," *IEEE Trans. Image Process.*, vol. 32, pp. 4472–4485, 2023.
- [38] Q. Liu, Q. Zhang, W. Liu, W. Chen, X. Liu, and X. Wang, "WSDS-GAN: A weak-strong dual supervised learning method for underwater image enhancement," *Pattern Recognit.*, vol. 143, Nov. 2023, Art. no. 109774.
- [39] K. Li et al., "Beyond single reference for training: Underwater image enhancement via comparative learning," *IEEE Trans. Circuits Syst. Video Technol.*, vol. 33, no. 6, pp. 2561–2576, Jun. 2023.
- [40] R. Liu, X. Fan, M. Zhu, M. Hou, and Z. Luo, "Real-world underwater enhancement: Challenges, benchmarks, and solutions under natural light," *IEEE Trans. Circuits Syst. Video Technol.*, vol. 30, no. 12, pp. 4861–4875, Dec. 2020.
- [41] G. Hou, N. Li, P. Zhuang, K. Li, H. Sun, and C. Li, "Non-uniform illumination underwater image restoration via illumination channel sparsity prior," *IEEE Trans. Circuits Syst. Video Technol.*, vol. 34, no. 2, pp. 799–814, Mar. 2024.
- [42] Y.-T. Peng, Y.-R. Chen, Z. Chen, J.-H. Wang, and S.-C. Huang, "Underwater image enhancement based on histogram-equalization approximation using physics-based dichromatic modeling," *Sensors*, vol. 22, no. 6, p. 2168, Mar. 2022.
- [43] H. Wang, S. Sun, and P. Ren, "Underwater color disparities: Cues for enhancing underwater images toward natural color consistencies," *IEEE Trans. Circuits Syst. Video Technol.*, vol. 34, no. 2, pp. 738–753, Mar. 2024.
- [44] S. An, L. Xu, Z. Deng, and H. Zhang, "HFM: A hybrid fusion method for underwater image enhancement," *Eng. Appl. Artif. Intell.*, vol. 127, Jan. 2024, Art. no. 107219.
- [45] M. Yu, L. Shen, Z. Wang, and X. Hua, "Task-friendly underwater image enhancement for machine vision applications," *IEEE Trans. Geosci. Remote Sens.*, vol. 62, 2024, Art. no. 5601014.
- [46] L. Ma et al., "Bilevel fast scene adaptation for low-light image enhancement," *Int. J. Comput. Vis.*, pp. 1–19, Oct. 2023, doi: [10.1007/s11263-023-01900-z](https://doi.org/10.1007/s11263-023-01900-z).
- [47] P. Hambarde, S. Murala, and A. Dhall, "UW-GAN: Single-image depth estimation and image enhancement for underwater images," *IEEE Trans. Instrum. Meas.*, vol. 70, pp. 1–12, 2021.
- [48] Y. Zheng, W. Chen, R. Lin, T. Zhao, and P. Le Callet, "UIF: An objective quality assessment for underwater image enhancement," *IEEE Trans. Image Process.*, vol. 31, pp. 5456–5468, 2022.
- [49] C. O. Ancuti, C. Ancuti, C. De Vleeschouwer, and P. Bekaert, "Color balance and fusion for underwater image enhancement," *IEEE Trans. Image Process.*, vol. 27, no. 1, pp. 379–393, Jan. 2018.
- [50] W. Zhang et al., "Underwater image enhancement via weighted wavelet visual perception fusion," *IEEE Trans. Circuits Syst. Video Technol.*, vol. 34, no. 4, pp. 2469–2483, Apr. 2024.
- [51] Y. Kang, Q. Jiang, C. Li, W. Ren, H. Liu, and P. Wang, "A perception-aware decomposition and fusion framework for underwater image enhancement," *IEEE Trans. Circuits Syst. Video Technol.*, vol. 33, no. 3, pp. 988–1002, Mar. 2023.
- [52] S. Liu, H. Fan, S. Lin, Q. Wang, N. Ding, and Y. Tang, "Adaptive learning attention network for underwater image enhancement," *IEEE Robot. Autom. Lett.*, vol. 7, no. 2, pp. 5326–5333, Apr. 2022.
- [53] C. O. Ancuti, C. Ancuti, C. De Vleeschouwer, and M. Sbert, "Color channel compensation (3C): A fundamental pre-processing step for image enhancement," *IEEE Trans. Image Process.*, vol. 29, pp. 2653–2665, 2020.
- [54] H. Yu, X. Li, Q. Lou, and L. Yan, "Underwater image enhancement based on color-line model and homomorphic filtering," *Signal, Image Video Process.*, vol. 16, no. 1, pp. 83–91, Feb. 2022.
- [55] Y.-T. Peng and P. C. Cosman, "Underwater image restoration based on image blurriness and light absorption," *IEEE Trans. Image Process.*, vol. 26, no. 4, pp. 1579–1594, Apr. 2017.
- [56] X. Ding, Y. Wang, and X. Fu, "An image dehazing approach with adaptive color constancy for poor visible conditions," *IEEE Geosci. Remote Sens. Lett.*, vol. 19, pp. 1–5, 2022.
- [57] Z. Liang, X. Ding, Z. Mi, Y. Wang, and X. Fu, "Effective polarization-based image dehazing with regularization constraint," *IEEE Geosci. Remote Sens. Lett.*, vol. 19, pp. 1–5, 2022.
- [58] R.-Q. Wu, Z.-P. Duan, C.-L. Guo, Z. Chai, and C. Li, "RIDCP: Revitalizing real image dehazing via high-quality codebook priors," in *Proc. IEEE/CVF Conf. Comput. Vis. Pattern Recognit. (CVPR)*, Jun. 2023, pp. 22282–22291.
- [59] X. Lv, T. Xiang, Y. Yang, and H. Liu, "Blind dehazed image quality assessment: A deep CNN-based approach," *IEEE Trans. Multimedia*, vol. 25, pp. 9410–9424, 2023.
- [60] Z. Fu, W. Wang, Y. Huang, X. Ding, and K.-K. Ma, "Uncertainty inspired underwater image enhancement," in *Proc. IEEE Conf. Eur. Conf. Comput. Vis.*, Oct. 2022, pp. 465–482.
- [61] J. Zhou, D. Zhang, and W. Zhang, "Underwater image enhancement method via multi-feature prior fusion," *Appl. Intell.*, vol. 52, no. 14, pp. 16435–16457, Mar. 2022.
- [62] M. Yin, X. Du, W. Liu, L. Yu, and Y. Xing, "Multiscale fusion algorithm for underwater image enhancement based on color preservation," *IEEE Sensors J.*, vol. 23, no. 7, pp. 7728–7740, Apr. 2023.
- [63] J. Liu, R. Lin, G. Wu, R. Liu, Z. Luo, and X. Fan, "CoCoNet: Coupled contrastive learning network with multi-level feature ensemble for multi-modality image fusion," *Int. J. Comput. Vis.*, vol. 132, no. 5, pp. 1748–1775, May 2024.
- [64] Q. Wu, L. Wang, K. N. Ngan, H. Li, F. Meng, and L. Xu, "Subjective and objective de-raining quality assessment towards authentic rain image," *IEEE Trans. Circuits Syst. Video Technol.*, vol. 30, no. 11, pp. 3883–3897, Nov. 2020.
- [65] R. Ma, Q. Wu, K. N. Ngan, H. Li, F. Meng, and L. Xu, "Forgetting to remember: A scalable incremental learning framework for cross-task blind image quality assessment," *IEEE Trans. Multimedia*, vol. 25, pp. 8817–8827, 2023.
- [66] L. Dong, W. Zhang, and W. Xu, "Underwater image enhancement via integrated RGB and LAB color models," *Signal Process., Image Commun.*, vol. 104, May 2022, Art. no. 116684.
- [67] K. Z. M. Azmi, A. S. A. Ghani, Z. M. Yusof, and Z. Ibrahim, "Natural-based underwater image color enhancement through fusion of swarm-intelligence algorithm," *Appl. Soft Comput.*, vol. 85, Dec. 2019, Art. no. 105810.
- [68] Y. Wang et al., "An imaging-inspired no-reference underwater color image quality assessment metric," *Comput. Electr. Eng.*, vol. 70, pp. 904–913, Aug. 2018.



Weidong Zhang (Senior Member, IEEE) received the Ph.D. degree in information and communication engineering from the School of Information Science and Technology, Dalian Maritime University, Dalian, China, in June 2022. He is currently a Post-Doctoral Fellow with the Postdoctoral Innovation Practice Base, Henan Institute of Science and Technology; the Postdoctoral Workstation, Henan Bainong Seed Industry Company Ltd.; and the College of Electrical and Information Engineering, Zhengzhou University. He is also a Full Professor with the School of

Information Engineering, Henan Institute of Science and Technology. He is also the Leader of the Institute of Computer Applications, Henan Institute of Science and Technology. He has published over 60 journal/conference papers on IEEE TRANSACTIONS ON IMAGE PROCESSING, IEEE TRANSACTIONS ON CIRCUITS AND SYSTEMS FOR VIDEO TECHNOLOGY, IEEE TRANSACTIONS ON GEOSCIENCE AND REMOTE SENSING, and AAAI. His current research interests include image restoration, intelligent agriculture, and deep learning. He is a Senior Member of CCF.



Lei Cai received the Ph.D. degree in control science and engineering from Air Force Engineering University, Xi'an, China, in 2009, and the degree from the Postdoctoral Mobile Station of Control Science and Engineering, Shandong University, in 2012. He is currently a Professor with the School of Artificial Intelligence, Henan Institute of Science and Technology. He has published over 40 journal/conference papers on IEEE TRANSACTIONS ON INDUSTRIAL INFORMATICS, IJARS, and *Robotica*. His current research interests include image processing, pattern recognition, light field reconstruction, and multi-agent adaptive coordination.



Qingmin Liu is currently pursuing the M.S. degree with the School of Information Engineering, Henan Institute of Science and Technology, Xinxiang, China. She is a member of the Institute of Computer Applications, Henan Institute of Science and Technology. Her research interests include image restoration and image enhancement.



Yikun Feng received the Master of Science degree from the University of Reading, U.K., in 2020. He is currently pursuing the Ph.D. degree in management with the Adam Smith Business School, University of Glasgow, U.K. His current research interests in the field of computer science are deep learning, decision support systems, and multi-task learning.



Peixian Zhuang (Member, IEEE) received the Ph.D. degree from the School of Informatics, Xiamen University, Xiamen, China, in 2016. From 2017 to 2020, he was a Lecturer and a Master's Supervisor with the School of Electronics and Information Engineering, Nanjing University of Information Science and Technology, Nanjing, China. From 2020 to 2022, he was a Post-Doctoral Fellow and an Assistant Research Fellow with the Department of Automation, Tsinghua University, Beijing, China. He is currently an Associate Professor with the Key Laboratory of Knowledge Education, School of Automation and Electrical Engineering, University of Science and Technology Beijing, Beijing. His research interests include sparse representation, Bayesian hierarchical modeling, deep learning, and calcium signal processing.